Simple mechanosense and response of cilia motion reveal the intrinsic habits of ciliates

Takuya Ohmura[a,1], Yukinori Nishigami[a,1], Atsushi Taniguchi[b], Shigenori Nonaka[b], Junichi Manabe[c], Takuji Ishikawa[c], and Masatoshi Ichikawa[a,2]

[a]Department of Physics, Kyoto University, Sakyo, Kyoto 606-8502, Japan; [b]Laboratory for Spatiotemporal Regulations, National Institute for Basic Biology, Okazaki 444-8585, Japan; and [c]Graduate School of Engineering, Tohoku University, Aoba, Sendai 980-8579, Japan

Edited by David A. Weitz, Harvard University, Cambridge, MA, and approved February 20, 2018 (received for review October 19, 2017)

An important habit of ciliates, namely, their behavioral preference for walls, is revealed through experiments and hydrodynamic simulations. A simple mechanical response of individual ciliary beating (i.e., the beating is stalled by the cilium contacting a wall) can solely determine the sliding motion of the ciliate along the wall and result in a wall-preferring behavior. Considering ciliate ethology, this mechanosensing system is likely an advantage in the single cell's ability to locate nutrition. In other words, ciliates can skillfully use both the sliding motion to feed on a surface and the traveling motion in bulk water to locate new surfaces according to the single "swimming" mission.

ciliates | mechanosense of cilia | swimming motility

Microorganisms play crucial roles in ecosystems and are essential to life on Earth (1–5). Eukaryotic unicellular microorganisms (i.e., protists) are dominant microorganisms in aquatic ecosystems (6–10). One class of protists, ciliates, exhibits a rapid translational swimming motion. Ciliates have a large number of hair-like organelles, termed cilia, that beat around the whole body to induce thrust force. While the remarkable activity of ciliates is usually observed in bulk water (11–15), they frequently accumulate on air/fluid and solid/fluid interfaces in nature (16–20). Although these two major characteristics (i.e., sliding on surfaces and traveling rapidly in bulk water) are commonly recognized as instinctive behaviors, the mechanism of the sliding motion remains unclear. Ciliates likely have sensing systems to detect walls or external boundary conditions and have a response mechanism connected to the transition between the modes of motion. To our knowledge, the mechanisms of sensing and response have not been revealed; however, this "wall taxis system" must be integrated into the life strategies of ciliates.

Are there clues about these mechanisms in biological studies or any hints related to their behavior in biophysical and hydrodynamic studies? Recent progress in numerical analysis and simulation has revealed the swimming mechanisms of various water microorganisms (21, 22). Studies of the interactions between a swimmer and a wall have shown that pusher and puller swimmers accumulate on a nonslip wall boundary (23–31). Pusher, puller, and neutral swimmers are swimming styles categorized by hydrodynamic models for active swimmers. Pusher swimmers are driven by rear propellers (e.g., *Escherichia coli*) and show repulsive motions from the wall. Puller swimmers, which are driven by anterior flagella (e.g., *Chlamydomonas*), have been numerically analyzed to determine their attractive motions toward a wall. Finally, the neutral swimmer is used as a model for ciliates that represent a uniform driving force covering the swimmer surface, assuming that cilia are beating all over the cell surface, as in *Volvox* (32) and *Tetrahymena* (33). The trajectories of neutral swimmers near a wall have been analytically and numerically reported. A wall repels neutral swimmers. More specifically, the propelling direction of the swimmer orients its departure from the wall. This property inhibits the accumulation of neutral swimmers on the wall. Although a recent simulation study with numerous neutral swimmers reported the accumulation of swimmers near the wall due to collective hydrodynamic effects from the swimmers that exist in surrounding environment (26), this finding was not applicable to accumulation or wall-preferring behavior at the individual cell level. Hydrodynamic studies have not yet explained the behaviors of ciliates on a wall. Our motivation for understanding the deviation between model swimmers and real ciliates near a wall led us to observe *Tetrahymena pyriformis*, a model organism of ciliates (34).

The swimming behaviors of *T. pyriformis* in bulk water and near the bottom of a wall are shown in Fig. 1. *T. pyriformis* in bulk water passed across the observation window over several seconds (Fig. S2*A*), while *T. pyriformis* at the bottom region remained on the wall (Fig. 1*A*, Fig. S2*B*, and Movie S1). Tracking the motion of *T. pyriformis* over 2.0 s revealed straight trajectories in bulk and straight or rotational motion on the wall, as shown in Fig. S2, respectively. Almost all rotation directions of the cilia on the wall were the same as the normal vector of the glass surface. *T. pyriformis* remained for 26.8 ± 4.7 s (mean ± SEM, $n = 20$) on the glass coated with 2-methacryloyloxyethyl phosphorylcholine (MPC; an antiadhesion agent) and for 5.2 ± 1.1 s (mean ± SEM, $n = 20$) on the uncoated glass. This process was commonly observed on the top wall (when it existed) and on the side wall (Fig. 1*B* and Movie S2). The steady swimming angle measured from the observation on this side wall was 13.2° on average (Fig. 1*C*) and was distributed below 40.0°. The travel speed in bulk water (up to 100 μm from the bottom wall) was 281.4 $\mu m \cdot s^{-1}$ on average, the travel speed on the MPC-coated glass was 138.2 $\mu m \cdot s^{-1}$, and the travel speed on the uncoated glass plate was 64.9 $\mu m \cdot s^{-1}$ (Fig. 1*D*). The travel speeds on the MPC-coated glass bottom walls were 49.1% as fast as those in bulk water, while those

Significance

Single-celled microorganisms are important in ecosystems, and their behaviors impact the Earth's environments. To survive in harsh environments, these organisms frequently act as though exercising discretion. How do they achieve such intelligent behaviors? In this work, we focused on the accumulation of ciliates on solid/fluid interfaces, where they can obtain sufficient nutrients and a stable environment. This phenomenon is not described in the standard hydrodynamics of microswimmers. Our experiment and simulation revealed that simple principles, the anisotropic shape of the cell and the mechanosensing nature of cilia, induce the accumulation of ciliates on solid/fluid interfaces. The contribution of our work is that a simple response of the cellular apparatus and fluid dynamics explain the apparently clever behavior of ciliates.

Author contributions: T.I. and M.I. designed research; T.O. and Y.N. performed research; A.T., S.N., J.M., and T.I. contributed new reagents/analytic tools; T.O. and Y.N. analyzed data; and T.O., Y.N., and M.I. wrote the paper.

The authors declare no conflict of interest.

This article is a PNAS Direct Submission.

[1]T.O. and Y.N. contributed equally to this work.

[2]To whom correspondence should be addressed. Email: ichi@scphys.kyoto-u.ac.jp.

This article contains supporting information online at www.pnas.org/lookup/suppl/doi:10.1073/pnas.1718294115/-/DCSupplemental.

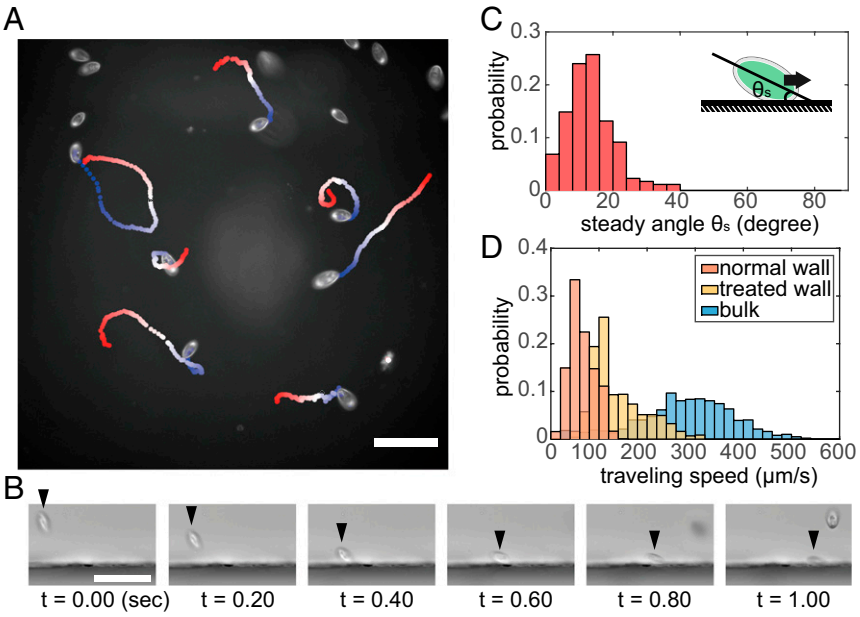

Fig. 1. Swimming behavior of individual *T. pyriformis* cells near walls. (*A*) Trajectories of *T. pyriformis* cells on a bottom wall. Most cells maintained their height during continuous swimming. (Scale bar, 100 μm.) (*B*) Snapshots of *T. pyriformis* swimming toward a side wall. After touching the wall, the cell slid along the wall. (Scale bar, 100 μm.) (*C*) Histogram of terminal or steady swimming angles θ_s between the wall and longitudinal axis of the cell body. (*Inset*) Angle was defined as shown. The arithmetic average of the angle was 13.2°. (*D*) Histogram of the propelling speeds of the cells in the bulk (yellow), near the treated glass wall (blue), and near the normal glass wall (red). While the mean speed in bulk was 281.4 μm·s^{-1}, the speed near the treated wall was 138.2 μm·s^{-1} and that near the normal wall was 64.9 μm·s^{-1}.

on the uncoated glass were 23.1% as fast as those in bulk water. These results confirm the interesting features of *T. pyriformis* on the wall; namely, *T. pyriformis* prefers a surface where it is not fixed but can slide. In this paper, "sliding" is defined as the observed motion adjacent to the wall. Considering the function of the MPC coat used to prevent the adhesion of proteins and biomacromolecules, the adhesive interaction strength between the substrate and the cilia was relatively inhibited on the coated surface. In addition, the sliding motions were observed on the antiadhesive glass for longer than on the normal glass. Thus, the adhesive bond pinning the cilia during long-duration beating is not the immediate cause of the sliding phenomenon. In other words, the pressure generated by other factors toward the wall should be investigated.

To examine the contributions and interactions of cilia and the wall according to their hydrodynamics, we visualized microscopic motion and flow fields around the single cells. Fig. 2*A* and Movie S3 show bright-field images of a single *T. pyriformis* from a 28° depression angle between the bottom glass plate and the cell. The surface of the bottom plate was identified based on the horizon between the direct image and the reflected virtual image. The estimated distances between the cell body and the wall were ∼3 μm, which is almost equal to the natural cilium length of *T. pyriformis*. The distances and motions of the cell reveal that *T. pyriformis* swam by contacting the wall only with its cilia. This observation was confirmed by fluorescent live cell imaging using the same perspective as in Fig. 2*B* and Movie S4, in which the cilia contacting the wall almost stopped beating (Fig. 2*B*, *Bottom*), whereas other intact cilia (e.g., those on the opposite side of the cell) continued beating (Fig. 2*B*, *Top*). Stoppage of the cilia beating on the wall side of the cell was also noted in phase-contrast observations from the bottom view. Fig. 2*C* shows numerous stopped cilia at the face of the bottom wall, where vertically standing cilia are visualized as black dots (indicated by red circles) in phase-contrast imaging (Movie S5). The beating speeds of the stopped cilia were estimated as 1/10th of those on the bulk side (Fig. 2*D*). Since the stopping of individual cilia occurred transiently with an average duration of 0.16 s at the single-cilium level, it is appropriate to refer to this phenomenon as a beating stall. In fact, the motion of probe beads indicated that the cilia in the upper and lateral areas of the cell paddled normally, whereas cilia at the bottom hardly paddled, as shown in the intensity and direction maps (Fig. 2 *E* and *F*). These experimental results indicate that the force generation was disturbed due to the presence of stalled cilia between the cell and the wall only. This phenomenon contributes to the sliding motion. Next, we incorporated the stalled phenomenon of cilium into a hydrodynamic cilium model to reveal the direct mechanism of the sliding motion of *T. pyriformis* on the wall.

Squirmer models have been used as mathematical models of swimming microswimmers (24–26, 35–41). We prescribe the mean shear stress generated by the beating flagella as acting tangentially. This model can approximate ciliary swimming by selecting a parameter to be neutral (i.e., the neutral swimmer). The details of the numerical setup are presented in *Materials and Methods* and Fig. S3. We simulate this model using the boundary element method to introduce the boundary condition mimicking the experimental results, where the "stop beating area" (SBA) is defined as the area beside a wall to reproduce the cilia that stop near the wall (Fig. 3*A*). The SBA range can be optimized to represent the stall ratio observed in the experiments. The parameter setup is shown in Fig. 3*B*. The boundary in this simulation did not contain lateral friction, which indicates that the boundary condition approximately represented the MPC-coated glass plate in the experiment.

First, we checked the motion of the model swimmers near the nonslip boundary wall without SBA (Fig. 4 *A* and *B* and Movies S6 and S7). Both spherical and ellipsoidal swimmers oriented their swimming direction against the wall, as observed in previous numerical and mathematical works (25, 26, 28). The spherical swimmer is a neutral swimmer, and the ellipsoidal swimmer mimics *T. pyriformis*'s shape. Without the SBA, neither swimmer exhibited a stable sliding mode on the wall, and both swam away from the wall under any initial conditions (Fig. S5). These behaviors are also shown in the graphs in Fig. 5 *E* and *F*, with $a = 0.0$, where the swimmer gradually oriented its direction near the wall. However, no stagnated or stable angle beside the wall was noted. Indeed, swimmers landing on the nonslip wall with the SBA did not take off. The range of the SBA was $a = 0.3$, and the wall was located at $z = -2$. Notably, the spherical swimmer in the simulation with the SBA stopped on the wall (Fig. 4*C* and Movie S8), whereas the ellipsoidal swimmer swam and slid adjacent to the wall (Fig. 4*D* and Movie S9). The latter is a qualitative representation of the sliding motion on the wall observed in the experiments. The trajectories and swimming angles of the swimmers with the SBA are shown in Fig. S4. The swimming angle of the spherical swimmer became perpendicular to the wall, and the translational (x direction) motion stopped (Fig. S4*A*). The swimming angle of the ellipsoidal swimmer converged to a certain angle and, after colliding, continued to slide on the wall (Fig. S4*B*). The terminal angle of the ellipsoidal swimmer was 11.9°, while that of the

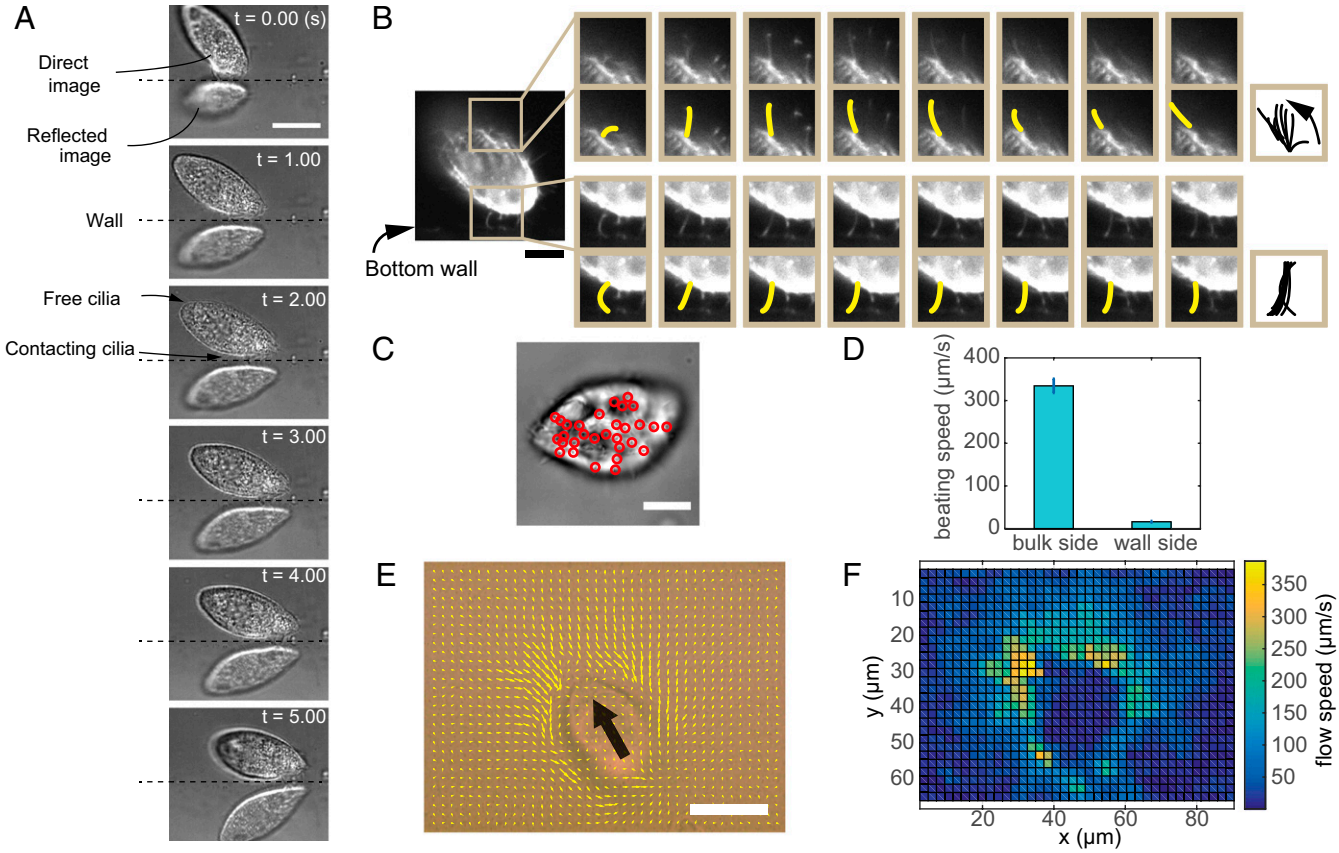

Fig. 2. Beating status of *T. pyriformis* cilia near the glass substrate. (*A*) Snapshots of *T. pyriformis* contacting the glass plate. The cell repeatedly touched and slid on the wall. (Scale bar, 20 μm.) (*B*) Snapshots of ciliary beating. (*Top*) Normal beat. (*Bottom*) Sticking beat touching the wall. The snapshots were taken at 10-ms intervals. (Scale bar, 10 μm.) (*C*) Snapshot of a cell swimming adjacent to a wall. The retained cilia standing perpendicular to the wall are identified as black areas in phase-contrast microscopy. The black points indicated by red circles are cilia stopping their stroke in several frames around the picture. (Scale bar, 10 μm.) (*D*) Comparison of the beating speeds in the bulk with those near the wall. The beating speeds of the cilia in bulk were estimated from the beating frequencies, and the mean cilia length was 3.2 μm (20 individual cilia). The beating speeds of the cilia contacting the wall were measured at the black points, as shown in *C*. (*E*) Flow field around the swimming cell was estimated by PIV analysis. The bold black arrow indicates the swimming direction of the cell. The analysis detected the motion of 0.5-μm silica beads at a height less than 1 μm from the bottom wall. (Scale bar, 20 μm.) (*F*) Intensity map of flow velocity in *E*. The velocity between the cell body and wall was very small but not zero.

spherical swimmer was 90.0°. The terminal angle in the ellipsoidal model was close to the experimental value of 13.2° at $a = 0.3$, confirming the experimental result shown in Fig. 1*C*. The terminal angles are not dependent on the initial entry angles $\theta_0 = 10°$ to 80° but, instead, are attributed to the SBA range $a = 0.00$ to 0.50, as noted in the supplementary graphs (Figs. S6 and S7, respectively). Summarizing the simulation results, the ellipsoidal swimmer slid on the wall at $a > 0.20$ and the terminal swimming angle varied as a function of a. In contrast, the spherical swimmer tended to have an angle of 90.0°. The adjacent motions of the swimmers were bifurcated by certain thresholds: $0.05 < a < 0.10$ for the spherical swimmer and $0.20 < a < 0.25$ for the ellipsoidal swimmer.

Discussion

We discuss the applicability of the model in terms of a qualitative comparison between the experimental and simulated behaviors. The actual body of *T. pyriformis* has an oral apparatus and a pear shape, which correspond to an anterior-posterior asymmetry and rotational asymmetry in the locomotive direction axis. Although the present simulation did not generate angular momentum along the axis, in the experiments, *T. pyriformis* did not exhibit rotational motion during its sliding motion. Therefore, the effects of asymmetry due to the oral apparatus are negligible for qualitative comparison in the present work. The anterior-posterior asymmetry of the shape requires more detailed study, but the present ellipsoidal shape can represent the experimental results semiquantitatively. Therefore, the crucial factor impacting the sliding motion must be the disruption of the spherical-ellipsoidal symmetry. In practical comparisons, the ellipsoidal swimmer slid on the wall in a manner similar to the behavior observed experimentally;

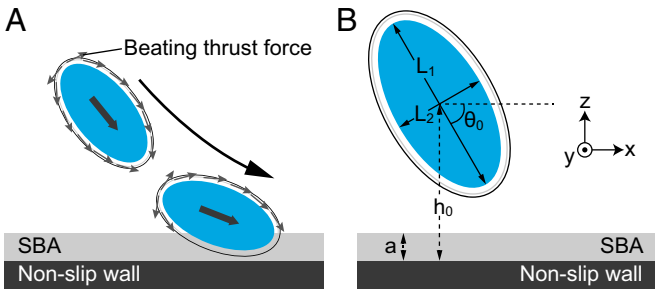

Fig. 3. Schematic illustrations of the simulation, indicating the geometries of the SBA and parameters. (*A*) Beating thrust forces (reaction force due to cilia strokes) along the surface driving the swimmer. We defined the SBA as the gray area on the bottom wall shown in the figure. If the surface is included within the SBA, the beating thrust force vanishes. (*B*) Parameter setup of the simulation. The shape of the force swimmer was determined by the ratio of the main axis length L_1 defined by the propelling direction to the waistline diameter L_2. The parameters were set as $L_1 = 2$ and $L_2 = 1$ or 2. $L_1/L_2 = 1$ corresponded to a spherical shape, and $L_1/L_2 = 2$ corresponded to an ellipsoidal shape. The SBA range was the defined length a. The initial angle was θ_0, and the initial height was fixed at $h_0 = 2.0$.

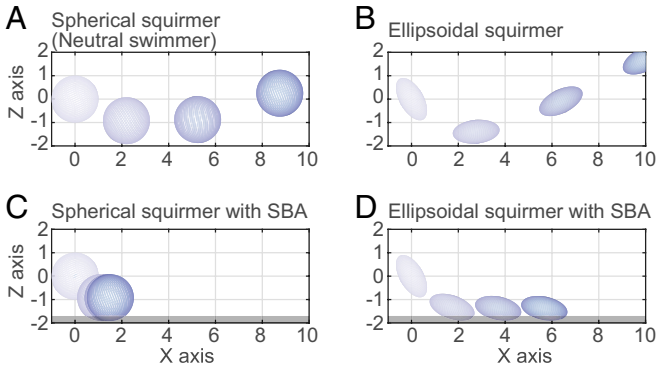

Fig. 4. Snapshots of simulation results reproducing swimmers approaching the wall. The initial angle is $\theta_0 = 60°$. The nonslip wall is located at $z = -2$. The gray area indicates the SBA. (*A*) $a = 0.0$; the spherical swimmer without SBA approached the wall and then swam away from the wall. (*B*) $a = 0.0$; the ellipsoidal swimmer without SBA swam away from the wall, similar to the spherical swimmer in *A*. (*C*) $a = 0.3$; the spherical swimmer with SBA did not swim away but stopped on the wall. (*D*) $a = 0.3$; the ellipsoidal swimmer with SBA swam adjacent to the wall.

that is, the terminal swimming angles of the cell body were close to each other: 13.2° (nose-down, experiment) and 11.9° (nose-down, numerical calculation for the ellipsoidal swimmer at $a = 0.3$), where the ratio of the projected area of cilia stopping at $a = 0.3$ was almost the same as that estimated by the experiment. In addition, the match between the swimming speeds of the experiments and the simulations was achieved. The speed-reducing ratios of the sliding speed on the wall V_w over the speed in the bulk V_b were $V_w/V_b = 0.49$ (experiment, on the MPC-coated glass) and $V_w/V_b = 0.55$ (simulation), which indicated that the boundary condition on the MPC-coated glass possibly had little lateral friction, inhibited the adhesion between cilia and the substrate, and was quantitatively represented by simulation with no lateral friction. In contrast, the ratio on the uncoated glass in the experiment was $V_w/V_b = 0.23$, and the difference must result from lateral friction. In addition, the force that the respective cilium experienced from the wall was at least 1.87 pN according to a comparison between the results of the experiment (~30 cilia stalled) and the simulation (56.2 pN was applied). In any event, the surface sliding phenomena of *T. pyriformis* accompanied by the stopping of ciliary beating were observed. According to the above-mentioned features, our simulation qualitatively reproduced actual ciliate swimming near the wall. Thus, the disruption of spherical-ellipsoidal symmetry and the cessation of ciliary beating near the wall are critical factors for ciliates swimming adjacent to a wall.

Since head-tail polar swimming direction(s) with angular velocity contribute primarily to determining whether a swimmer stops, slides, or departs from the wall, any torque balance that influences the swimmer and develops angular velocity should be considered. The causes of this torque are categorized into three patterns: hydrodynamic interaction, stopping of beating, and wall repulsion (Fig. 6). If the swimmer approaches the wall from the top left, the hydrodynamic interaction from the wall has a nose-up torque, and asymmetrical propelling force due to the stoppage of beating acts as a nose-down torque. Both torques act on both spherical and ellipsoidal swimmers. In contrast, wall repulsion gives rotational torque not to the spherical swimmer but to the ellipsoidal swimmer. Under this simplified scheme, the spherical swimmer touching the wall is given total torque from two factors without a balance point; thus, the swimming direction is downward when $a > 0.2$ and to the top right when $a < 0.15$ (Fig. S7). These values correspond to stop and departure, respectively. However, the torque from the wall repulsion additionally acts on the ellipsoidal swimmer, affecting the total torque with a stationary fixed point of a certain angle θ_m, $-90.0° < \theta_m < 0.0°$. Thus, the ellipsoidal swimmer could slide on the wall, and the adjacent swimmer was stable at a certain angle (Fig. 5 and Fig. S6).

Finally, we discuss the biological relevance and applicability of the present results through comparison with other species. One well-studied ciliate, *Paramecium caudatum*, usually exhibits a back-and-forth motion against the uncoated wall (Movie S11), which is caused by a mechanosensing system at the anterior region of the cell (14). However, with the MPC-coated glass, *P. caudatum* also showed sliding motion for a long time (Movie S12), as did *T. pyriformis*, which would arise from the same dynamics. Ciliates are known to exist at air/fluid and solid/fluid interfaces in nature because these interfaces provide biofilm scaffolds composed of diatoms, alga, bacteria, polysaccharides, and proteins (42–45). These components are favorite foods for ciliates (3, 9, 10). In the case of the water/air interface (WAI), Ferracci et al. (20) determined that *Tetrahymena* is also trapped at the WAI. However, the trapped cells did not stop their ciliary beating. This finding indicates that the cell does not have an SBA at the WAI, and the mechanisms of entrapment at the WAI will differ from those at the water/wall interface presented here. Adapting these facts to our results, the coupling of the mechanical and hydrodynamical responses allows ciliates to easily remain on solid interfaces, which is one of their preferred environments. This is a discovery of the ethology of ciliates accompanied by the mechanism coupling cilia motion and swimming behavior, and the finding also suggests why many ciliates have evolved ellipsoidal shapes. Spherical ciliates have a disadvantage in finding nutrients when sliding on surfaces. In the experiments, when *T. pyriformis* slid on a wall, its oral apparatus was located at the most appropriate position (i.e., close to the wall) (Fig. 2*A*). As for the

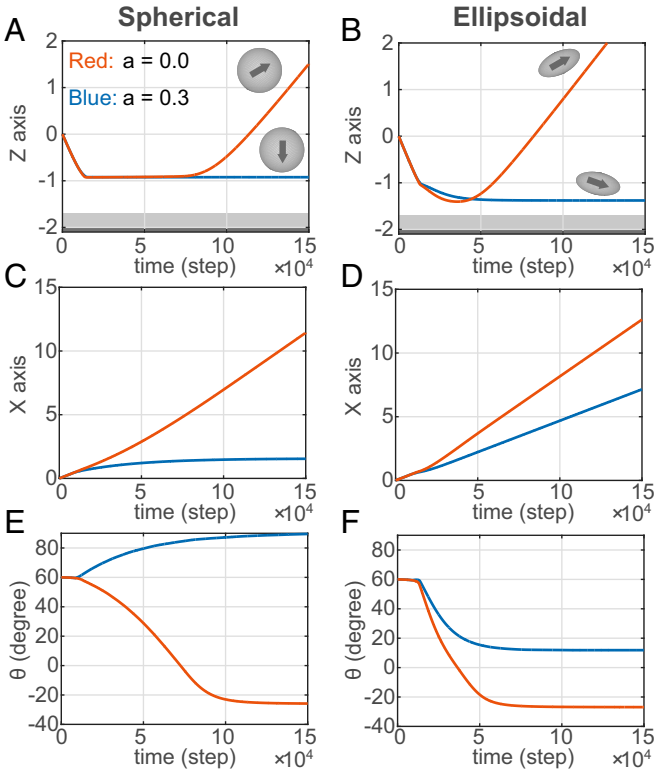

Fig. 5. Comparison of z and x positions and swimming angle. Red lines represent trajectories without the SBA, where length $a = 0.0$, and blue lines indicate $a = 0.3$. (*A*, *C*, and *E*) Spherical swimmer. (*B*, *D*, and *F*) Ellipsoidal swimmer. The gray area in *A* and *B* represents the SBA. From *A* and *B*, both the spherical and ellipsoidal swimmers showed similar changes in z position. From *C* and *D*, while the spherical swimmer stopped on the x axis when $a = 0.3$, the ellipsoidal swimmer stably slid on the wall. From *E* and *F*, the swimming angles indicate asymptotic values. The angles below 0.0° indicate swimmers swimming away from the wall. The terminal angle of the spherical swimmer was 90.0°, which corresponds to a swimmer oriented vertically against the wall. The terminal angle of the ellipsoidal swimmer was 11.9°.

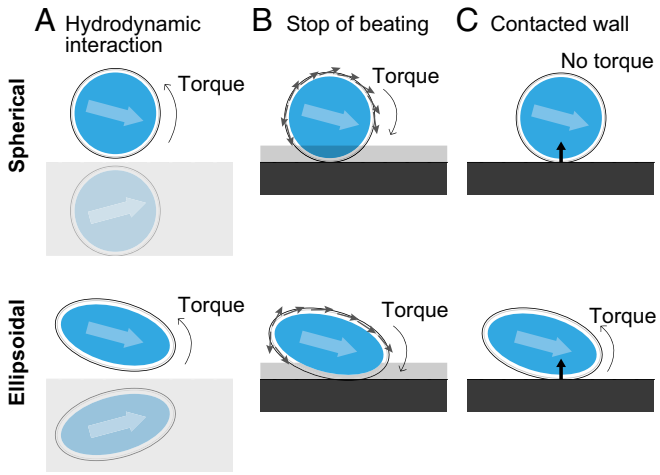

Fig. 6. Schematic illustrations of torques for a spherical swimmer (*Top*) and ellipsoidal swimmer (*Bottom*) approaching a wall from the left side. (*A*) Hydrodynamic interactions caused by the wall apply nose-up torques. (*B*) Stopping the cilia beating inside the SBA affects the total propelling force around the bodies, leading to asymmetry and nose-down torques. (*C*) Mechanical repulsion from the wall. The spherical swimmer experienced no torque, whereas the ellipsoidal swimmer experienced nose-up torque.

spherical swimmer, which was propelled by means of multiple flagella on the surface (*Volvox carteri*), it continued swimming near the top and bottom walls, which was explained by gyrotaxis (46), which has different dynamics from the observed phenomenon because the sliding motion of *T. pyriformis* arose without gravity.

In conclusion, we reveal that *T. pyriformis* swims adjacent to the wall using the mechanohydrodynamics of beating cilia, without cell adhesion, many-body effects (26), and chemotaxis. This phenomenon is essentially attributable to the ellipsoidal shape of the ciliate and the mechanosensing and response of the beating cilia against the attached surface. Although future biochemical investigations are required on the detailed mechanosense/response in the ciliary motion, the present results should be considered in analyses of the collective motion of ciliates and bioconvection (47, 48).

Materials and Methods

Preparation of *Tetrahymena pyriformis*. *T. pyriformis* was kindly gifted by Osamu Numata, University of Tsukuba, Tsukuba, Japan. The cells were cultured in growth medium [1.2% (wt/vol) Bacto Proteose Peptone (Becton, Dickinson and Company), 0.6% (wt/vol) Paticase (Kyokuto), and 0.2% (wt/vol) Bacto Yeast Extract (Becton, Dickinson and Company)] at room temperature (20–25 °C) with aeration (e-AIR6000WB; GEX). Serial transfer of the cells was performed twice per week. Before observation, the cells in midlog phase were washed three times with observation solution [10 mM 3-(N-morpholino)propanesulfonic acid/Tris (pH 7.2), 1 mM KCl, 1 mM NaCl, and 1 mM $CaCl_2$] (49) and equilibrated with observation solution for more than 1 h before observation.

Bright- and Dark-Field Observations of *T. pyriformis* at Perpendicular and Parallel Angles. To prevent nonspecific binding between the cells and the surface of the cover glasses, the cover glasses (thickness no. 1, 30 × 40 mm; Matsunami) were coated with MPC polymer (Lipidure-CM5206; NOF Corporation). Specifically, MPC polymer was dissolved in ethanol to a final concentration of 0.5% (wt/vol), and 20 μL of MPC polymer solution was placed on the cover glass. To dry the coating solution, the glass was left at room temperature for more than 2 h. The observation solution containing *T. pyriformis* was deposited between MPC-coated cover glasses with a spacer [a silicone sheet (thickness of 400 μm) with a square hole (side length of 10 mm)]. *T. pyriformis* was observed and recorded using bright-field and dark-field inverted microscopy (Eclipse Ti; Nikon) with an sCMOS camera (ORCA-Flash4.0; Hamamatsu). To observe side views of *T. pyriformis* in a bright field, the cover glasses (thickness no. 1; Matsunami) were substituted for silicone spacers, and *T. pyriformis* on the glass spacers was observed using the methods described above.

Fluorescence and Bright-Field Observations of *T. pyriformis* at a Low Angle. To acquire low-angle fluorescence images of *T. pyriformis* attached to the glass surface, observations were performed as described previously (50). In brief, a light-sheet, which was used as an excitation light, was generated by a line-scanning laser beam (FV10-LD559; Olympus) (Fig. S1 *A* and *B*) using a confocal laser-scanning microscope (FV1000; Olympus). An sCMOS camera (ORCA-Flash4.0) with an optical axis orthogonal to the plane of the excitation light was used for image acquisition. A cover glass was set at an angle of 28° to the optical axis (Fig. S1C). After the chamber unit was filled with observation solution, *T. pyriformis* was stained for 10 min in observation solution containing 10 μg/mL CellMask Orange plasma membrane stain (Molecular Probes) and washed three times with observation solution. The organism was then added to the chamber unit, and the cells on the glass were observed through a bandpass filter (BA570-625HQ; Olympus). In bright-field observation, a halogen lamp (LG-PS2; Olympus) was used as the light source (Fig. S1*D*).

Particle Image Velocimetry Analysis. The flow velocity field and speed intensity around the cell body (Fig. 2 *E* and *F*) were obtained using an open-source MATLAB code (PIVlab) (51). The raw movie was recorded at 2,000 fps (Movie S10), and the snapshots at a 1.5-ms interval were used for particle image velocimetry (PIV) analysis.

Three Surfaces in Our Numerical Model. In this calculation, there are three defined boundaries: body surface, stress surface, and cilia surface (Fig. S3*B*). The body surface is rigid and has a nonslip boundary condition. The shape is spherical or prolate ellipsoidal. An actual ciliate is anisotropic in shape, as in the prolate ellipsoid. The diameter of the spherical surface is 2.0. The major and minor lengths of the ellipsoidal surface are 2.0 and 1.0, respectively. The cilia surface is located outside the body surface. The length of the cilia in this model is fixed at 0.1, which is estimated from the actual cells. The stress surface is defined to reproduce the stress force of ciliary beating per unit area. Usually, the squirmer model is given by a velocity field on the surface, but we used a thrust stress force instead of a velocity field to precisely reproduce the actual beating (Fig. S3*A*). The stress surface is located between the body surface and the cilia surface (Fig. S3*D*). We used a boundary element method for numerical calculation (21). All surfaces are discretized by 162 material points far from the boundary and 2,562 material points near the boundary. The length unit is normalized by the radius of the spherical swimmer (i.e., 1.0).

Numerical Methods. We derived a numerical method assuming $\boldsymbol{x}=(x,y,z)$ as an observation point and $\boldsymbol{y}$ as a source point. Assuming the surface traction acting on the cell surface $\boldsymbol{q}(\boldsymbol{y})$ and the thrust force per unit area $\boldsymbol{F}(\boldsymbol{x})$, the flow field is given by a boundary integral equation (52):

$$\boldsymbol{u}(\boldsymbol{x})=\boldsymbol{u}_\infty(\boldsymbol{x})-\int \boldsymbol{J}_0(\boldsymbol{x},\boldsymbol{y})\cdot\boldsymbol{q}(\boldsymbol{y})\mathrm{d}S_b(\boldsymbol{y})-\int \boldsymbol{J}_0(\boldsymbol{x},\boldsymbol{y})\cdot\boldsymbol{F}(\boldsymbol{y})\mathrm{d}S_c(\boldsymbol{y}), \quad [1]$$

where $\mathrm{d}S_b$ and $\mathrm{d}S_c$ are the body surface and the stress surface, respectively. $\boldsymbol{J}_0(\boldsymbol{x},\boldsymbol{y})=1/8\pi\mu(\delta_{ij}/r+r_ir_j/r^3)$ represents the single-layer potentials of Green's function, which is the second-order tensor called the Oseen tensor, and $\boldsymbol{u}_\infty(\boldsymbol{x})$ expresses the external flow field. In this paper, $\boldsymbol{u}_\infty(\boldsymbol{x})$ is defined as zero.

Next, the flow field on the body surface $\boldsymbol{u}_S(\boldsymbol{x})$ is determined using the velocity of the mass $\boldsymbol{U}$ and the turning angular velocity $\boldsymbol{\Omega}$ considering the nonslip boundary condition. The kinetic velocity on the body surface is described as follows:

$$\boldsymbol{u}_S(\boldsymbol{x})=\boldsymbol{U}+\boldsymbol{\Omega}\wedge(\boldsymbol{y}-\boldsymbol{X}_0). \quad [2]$$

Here, the external force $\boldsymbol{F}$ and torque $\boldsymbol{T}$ are decided as boundary conditions:

$$\boldsymbol{F}=\int \boldsymbol{q}(\boldsymbol{y})\mathrm{d}S_b(\boldsymbol{y})=\int \boldsymbol{F}(\boldsymbol{y})\mathrm{d}S_c(\boldsymbol{y}). \quad [3]$$

$$\boldsymbol{T}=\int \boldsymbol{q}(\boldsymbol{y})\wedge(\boldsymbol{y}-\boldsymbol{X}_0)\mathrm{d}S_b(\boldsymbol{y})=\int \boldsymbol{F}(\boldsymbol{y})\wedge(\boldsymbol{y}-\boldsymbol{X}_0)\mathrm{d}S_c(\boldsymbol{y}). \quad [4]$$

By solving the simultaneous Eqs. **1**–**4**, $\boldsymbol{U},\boldsymbol{\Omega}$, and $\boldsymbol{q}(\boldsymbol{x})$ can be derived. Once the translational and angular velocities are obtained, the material points are updated by a fourth-order Adams–Bashforth method. The time step was set to $\Delta t=1.0\times10^{-4}$. The swimming speed at infinity U and the viscosity μ were fixed to $U=\mu=1.0$. Fig. S3*C* shows the streamlines of this model. The swimmer has a dipole-like velocity potential, which is the property of a neutral swimmer.

Wall Interactions. Assuming that a wall is a rigid, nonslip boundary, the swimmer experiences forces and torques from the wall. First, we considered the hydrodynamic interactions with the wall. The hydrodynamic interactions

are derived using a modified Oseen tensor (41). The Oseen tensor J_0 in the second term of Eq. **1** is changed to

$$\boldsymbol{J}(\boldsymbol{x},\boldsymbol{y}) = \boldsymbol{J}_0(\boldsymbol{x},\boldsymbol{y}) - \boldsymbol{J}_w(\boldsymbol{x},\boldsymbol{y}'),$$

$$\boldsymbol{J}_w(\boldsymbol{x},\boldsymbol{y}') = -\boldsymbol{J}_0(\boldsymbol{x},\boldsymbol{y}') + 2h^2\boldsymbol{J}_D(\boldsymbol{x},\boldsymbol{y}') - 2h\boldsymbol{J}_{SD}(\boldsymbol{x},\boldsymbol{y}'),$$

where h is the height at the center of the swimmer:

$$\boldsymbol{J}_D(\boldsymbol{x},\boldsymbol{y}') = (1-2\delta_{i3})\left(\frac{\delta_{ij}}{r'^3} + \frac{3r'_i r'_j}{r'^5}\right).$$

$$\boldsymbol{J}_{SD}(\boldsymbol{x},\boldsymbol{y}') = (1-2\delta_{i3})\left(\frac{\delta_{ij}r'_3 - \delta_{i3}r'_j + \delta_{j3}r'_i}{r'^3} - \frac{3r'_i r'_j r'_3}{r'^5}\right).$$

Next, we considered the repulsion from the rigid wall. When the swimmer is approaching the wall, the swimmer sometimes overlaps the wall. Therefore, the repulsion force and torque from the collision are added to Eqs. **3** and **4**:

$$\boldsymbol{F}_{rep} = \int \boldsymbol{F'}_{rep}(\boldsymbol{y})\mathrm{d}S_a(\boldsymbol{y}),$$

$$\boldsymbol{T}_{rep} = \int \boldsymbol{F'}_{rep}(\boldsymbol{y}) \wedge (\boldsymbol{y} - \boldsymbol{X}_0)\mathrm{d}S_a(\boldsymbol{y}),$$

where $\boldsymbol{F'}_{rep}(\boldsymbol{y})$ is expressed as the repulsion force between the cilia and the wall per unit area. To reproduce the interaction between the cilia and the wall, we assume that the cilia are linear springs and $\boldsymbol{F'}_{rep}(\boldsymbol{y}) = kl_c(\boldsymbol{y})\boldsymbol{e}_z$, where $l_c(\boldsymbol{y})$ is the shrinking length of the cilia, k is the spring constant, and S_a is the area of cilia touching the wall. We do not consider friction with the wall in this calculation. Therefore, the repulsion force has only a z-axis component.

Finally, we introduced a boundary condition. To reproduce the stopping of the cilia near the wall, we defined the SBA as the gray area on the bottom wall shown in Fig. 3*A*. The ciliary beating inside the SBA stops; thus, the thrust force $\boldsymbol{F}(\boldsymbol{y})$ near the wall vanishes. We define length a as the parameter of the SBA range in Fig. 3*B*. When the ellipsoidal swimmer touched the bottom wall at a swimming angle of 11.9°, the ratio of the projected area of cilia stopping at $a = 0.3$ was 69.9%, which almost corresponds to the value estimated by the experiment.

ACKNOWLEDGMENTS. We thank Prof. Osamu Numata and Dr. Kentaro Nakano (University of Tsukuba) for the gift of *T. pyriformis*. This work was supported by Grant 17-503 of the NIBB Collaborative Research Program. *Paramecium* cells used in this study were provided by the Symbiosis Laboratory at Yamaguchi University with support, in part, from the National Bio-Resource Project of the Japan Agency for Medical Research and Development. This work was also supported by Japan Society for the Promotion of Science KAKENHI Grants JP17J06827, JP17J10331, JP26707020, and JP25103012 and promoted by the MAthematics-based Creation of Science (MACS) program, Kyoto University.

1. Pomeroy L-R (1974) The ocean's food web, a changing paradigm. *Bioscience* 24: 499–504.
2. Azam F, et al. (1983) The ecological role of water-column microbes in the sea. *Mar Ecol Prog Ser* 10:257–263.
3. Wetzel R-G (2001) *Limnology: Lake and River Ecosystems* (Gulf Professional Publishing, Houston).
4. Fenchel T, Blackburn T-H, King G-M (2012) *Bacterial Biogeochemistry: The Ecophysiology of Mineral Cycling* (Academic, San Diego).
5. Kirchman D-L (2012) *Processes in Microbial Ecology* (Oxford Univ Press, Oxford).
6. Mitra A, et al. (2014) The role of mixotrophic protists in the biological carbon pump. *Biogeosciences* 11:995–1005.
7. Mitra A, et al. (2016) Defining planktonic protist functional groups on mechanisms for energy and nutrient acquisition: Incorporation of diverse mixotrophic strategies. *Protist* 167:106–120.
8. Ward B-A, Follows M-J (2016) Marine mixotrophy increases trophic transfer efficiency, mean organism size, and vertical carbon flux. *Proc Natl Acad Sci USA* 113:2958–2963.
9. Weisse T (2017) Functional diversity of aquatic ciliates. *Eur J Protistol* 61:331–358.
10. Weisse T, et al. (2016) Functional ecology of aquatic phagotrophic protists–Concepts, limitations, and perspectives. *Eur J Protistol* 55:50–74.
11. Jennings H-S (1904) The behavior of paramecium. Additional features and general relations. *J Comp Neurol Psychol* 14:441–510.
12. Ishikawa T, Hota M (2006) Interaction of two swimming Paramecia. *J Exp Biol* 209: 4452–4463.
13. Funfak A, et al. (2015) Paramecium swimming and ciliary beating patterns: A study on four RNA interference mutations. *Integr Biol* 7:90–100.
14. Jana S, Eddins A, Spoon C, Jung S (2015) Somersault of Paramecium in extremely confined environments. *Sci Rep* 5:13148.
15. Kunita I, et al. (2016) A ciliate memorizes the geometry of a swimming arena. *J R Soc Interface* 13:20160155.
16. Fenchel T (1968) The ecology of marine microbenthos. II. The food of marine benthic ciliates. *Ophelia* 5:73–121.
17. Fenchel T (1969) The ecology of marine microbenthos. IV. Structure and function of the benthic ecosystem, its chemical and physical factors and the microfauna communities with special reference to the ciliated protozoa. *Ophelia* 6:1–182.
18. Fenchel T (1987) *Ecology of Protozoa* (Springer, Berlin).
19. Fenchel T (1992) What can ecologists learn from microbes: Life beneath a square centimetre of sediment surface. *Funct Ecol* 6:499–507.
20. Ferracci J, et al. (2013) Entrapment of ciliates at the water-air interface. *PLoS One* 8: e75238.
21. Omori T, Ishikawa T (2016) Upward swimming of a sperm cell in shear flow. *Phys Rev E* 93:032402.
22. Kinosita Y, Uchida N, Nakane D, Nishizaka T (2016) Direct observation of rotation and steps of the archaellum in the swimming halophilic archaeon Halobacterium salinarum. *Nat Microbiol* 1:16148.
23. Kantsler V, Dunkel J, Polin M, Goldstein R-E (2013) Ciliary contact interactions dominate surface scattering of swimming eukaryotes. *Proc Natl Acad Sci USA* 110: 1187–1192.
24. Wang S, Ardekani A-M (2013) Swimming of a model ciliate near an air-liquid interface. *Phys Rev E Stat Nonlin Soft Matter Phys* 87:063010.
25. Ishimoto K, Gaffney E-A (2013) Squirmer dynamics near a boundary. *Phys Rev E Stat Nonlin Soft Matter Phys* 88:062702.
26. Li G-J, Ardekani A-M (2014) Hydrodynamic interaction of microswimmers near a wall. *Phys Rev E Stat Nonlin Soft Matter Phys* 90:013010.
27. Berke A-P, Turner L, Berg H-C, Lauga E (2008) Hydrodynamic attraction of swimming microorganisms by surfaces. *Phys Rev Lett* 101:038102.
28. Spagnolie S-E, Lauga E (2012) Hydrodynamics of self-propulsion near a boundary: Predictions and accuracy of far-field approximations. *J Fluid Mech* 700:105–147.
29. Ishikawa T (2009) Suspension biomechanics of swimming microbes. *J R Soc Interface* 6: 815–834.
30. Schaar K, Zöttl A, Stark H (2015) Detention times of microswimmers close to surfaces: Influence of hydrodynamic interactions and noise. *Phys Rev Lett* 115:038101.
31. Llopis I, Pagonabarraga I (2010) Hydrodynamic interactions in squirmer motion: Swimming with a neighbour and close to a wall. *J Nonnewton Fluid Mech* 165: 946–952.
32. Drescher K, Goldstein R-E, Michel N, Polin M, Tuval I (2010) Direct measurement of the flow field around swimming microorganisms. *Phys Rev Lett* 105:168101.
33. Ferracci J (2013) Hydrodynamics of ciliates at the air-liquid interface. PhD thesis (Tohoku University, Sendai, Japan).
34. Hutton J-C (1997) Tetrahymena: The key to the genetic analysis of the regulated pathway of polypeptide secretion? *Proc Natl Acad Sci USA* 94:10490–10492.
35. Lighthill M-J (1952) On the squirming motion of nearly spherical deformable bodies through liquids at very small Reynolds numbers. *Commun Pure Appl Math* 5:109–118.
36. Ishikawa T, Simmonds M-P, Pedley T-J (2006) Hydrodynamic interaction of two swimming model micro-organisms. *J Fluid Mech* 568:119–160.
37. Thutupalli S, Seemann R, Herminghaus S (2011) Swarming behavior of simple model squirmers. *New J Phys* 13:073021.
38. Downton M-T, Stark H (2009) Simulation of a model microswimmer. *J Phys Condens Matter* 21:204101.
39. Lauga E, Powers T-R (2009) The hydrodynamics of swimming microorganisms. *Rep Prog Phys* 72:096601.
40. Blake J-R (1971) A spherical envelope approach to ciliary propulsion. *J Fluid Mech* 46: 199–208.
41. Blake J-R (1971) A note on the image system for a Stokeslet in a no-slip boundary. *Math Proc Camb Philos Soc* 70:303–310.
42. Solano C, et al. (2002) Genetic analysis of Salmonella enteritidis biofilm formation: Critical role of cellulose. *Mol Microbiol* 43:793–808.
43. Friedman L, Kolter R (2004) Genes involved in matrix formation in Pseudomonas aeruginosa PA14 biofilms. *Mol Microbiol* 51:675–690.
44. Martí S, et al. (2011) Biofilm formation at the solid-liquid and air-liquid interfaces by Acinetobacter species. *BMC Res Notes* 4:5.
45. Constantin O (2009) Bacterial biofilms formation at air liquid interfaces. *Innov Rom Food Biotechnol* 5:18–22.
46. Drescher K, et al. (2009) Dancing volvox: Hydrodynamic bound states of swimming algae. *Phys Rev Lett* 102:168101.
47. Kitsunezaki S, Komori R, Harumoto T (2007) Bioconvection and front formation of Paramecium tetraurelia. *Phys Rev E Stat Nonlin Soft Matter Phys* 76:046301.
48. Mogami Y, Yamane A, Gino A, Baba SA (2004) Bioconvective pattern formation of Tetrahymena under altered gravity. *J Exp Biol* 207:3349–3359.
49. Muto Y, Tanabe Y, Kawai K, Okano Y, Iio H (2011) Climacostol inhibits Tetrahymena motility and mitochondrial respiration. *Open Life Sci* 6:99–104.
50. Takao D, Taniguchi A, Takeda T, Sonobe S, Nonaka S (2012) High-speed imaging of amoeboid movements using light-sheet microscopy. *PLoS One* 7:e50846.
51. Thielicke W, Stamhuis E-J (2014) PIVlab–Towards user-friendly, affordable and accurate digital particle image velocimetry in MATLAB. *J Open Res Softw* 2:e30.
52. Pozrikidis C (1992) *Boundary Integral and Singularity Methods for Linearized Viscous Flow* (Cambridge Univ Press, Cambridge, UK).